A&A manuscript no.
(will be inserted by hand later)

Your thesaurus codes are:
11(11.09.1 M31; 11.14.1; 11.11.1)

ASTRONOMY
AND
ASTROPHYSICS
1.2.2008

N body simulations of the nucleus of M31

E. Emsellem[1,2] and F. Combes[3]

[1] European Southern Observatory, Karl-Schwarschild Strasse 2, D-85748 Garching b. München, Germany
[2] Sterrewacht Leiden, Postbus 9513, 2300 RA Leiden, The Netherlands
[3] Observatoire de Paris, DEMIRM, 61 av. de l'Observatoire, F-75014 Paris

accepted 14/01, 1997

Abstract. We test through stellar N-body simulations some scenarios to explain the dynamics of the peculiar nucleus of the Andromeda galaxy (M 31): although HST observations reveal a double nucleus morphology, the rotation field is almost symmetric around the bulge gravity centre and the velocity dispersion is off-centred. We show that any $m = 1$ perturbation has a very short life-time (a few 10^5 yr). Assuming that the bright peak (P1) is a cold stellar cluster infalling into the nucleus, and that the large central velocity gradient is due to a central dark mass (in the range 7 10^7–10^8 $M_\odot$), we obtain a reasonably good fit to the observations. However, if this cluster lies in the central 20 pc, we estimate the life-time of the cluster to be less than 0.5 Myr. The dynamical friction is more efficient than estimated by analytic formulae, and is essentially due to the deformation of the stellar cluster through the huge tidal forces provided by the black hole. We show that the cluster cannot be on a circular orbit around the centre if the nucleus hosts a massive black hole of a few 10^7 $M_\odot$, and finally provide some estimates of the kinematics as observed with HST.

Key words: galaxies: M 31 - galaxies: nuclei – galaxies: kinematic and dynamics

1. Introduction

Each new observational result concerning the nucleus of M 31 seems to deepen the mystery of its structure. This is mainly due to the improvement in the achieved spatial resolution of the photometric and spectroscopic data: the better resolved the object is, the more complex it appears. For any proposed physical mechanism which can quantitatively reproduce the observables, it is important to provide some specific predictions.

Send offprint requests to: E. Emsellem (email: eemselle@eso.org)

In this respect, the nucleus of M 31 is certainly an excellent laboratory to test our knowledge of galactic nuclei, as we can now optically resolve scales as small as 0.3 pc (e.g. HST or optically adaptive ground-based systems). Indeed, the numerous studies achieved on this object revealed a puzzling complexity.

M 31's nucleus is a compact stellar system with an average ellipticity of $\langle\epsilon\rangle \sim 0.4$. Asymmetries in its major-axis surface brightness profile (in the visible) were already observed in 1974 by Light et al., and subsequently understood using the pre COSTAR HST data as a double component nucleus (Lauer et al. 1993). In the V band, the fainter peak (P2) is almost coincident with the centre of the bulge isophotes, as the brightest one (P1) is located at about 0.″5 ($\sim$ 1.8 pc for a distance to M 31 of 0.77 Mpc) from P2 roughly along the major-axis. At 175 nm however, P2 is the brightest point, with P1 having an UV upturn similar to its surroundings (King et al. 1995).

In 1960, Lallemand et al. obtained spectrograms of the central region of M 31 and detected the rapid rotation of its nucleus, concluding that it is a dynamically independent structure. This was confirmed by Kormendy (1988) and Dressler & Richstone (1988) by long-slit spectroscopy with CCD detectors. Both studies suggest the presence of a central dark mass of the order of 10^7 $M_\odot$ in the centre of the nucleus which would account for the high value of the central velocity and velocity dispersion gradients.

Sub-arcsecond velocity and dispersion maps were obtained with the TIGER spectrograph by Bacon et al. (1994, hereafter BEMN94) which uncovered more asymmetries (already traced in previous published data): the velocity field is nearly symmetric about a point V_0 located very close to P2 (0.″05 according to Lauer et al. 1993), but the maximum S of the stellar velocity dispersion roughly corresponds to the symmetric point of P1 with respect to P2 (see Fig. 26 of BEMN94).

Different interpretations have been proposed to explain the observed photometric and dynamical asymmetries in the nucleus of M 31 (see Sect. 2 and references therein), but they each encounter severe problems. Some questions

remain open, such as the actual efficiency of dynamical friction for an external body falling into the nucleus, the life-time of $m = 1$ perturbations, or the amount of dynamical perturbation on the nucleus itself; we try here to answer these questions through N body simulations. In this paper, we concentrate on one of the proposed mechanism, namely that P1 corresponds to a stellar cluster falling into the potential well of the nucleus, hosting a massive black hole. In a companion paper, we will examine whether a central black hole is unavoidable, or the presence of a nuclear bar could account for the observational data.

We summarize and comment the alternatives already discussed by different authors in Sect. 2. In Sect. 3 we describe the N body code we used as well as the initial conditions of the different experiments. The results are discussed in Sect. 4. In Sect. 5, we present and discuss our attempts to fit the observables using different assumptions. The general discussion and conclusions are given in Sect. 6.

2. Different mechanisms

The M31 nucleus is an object of peculiar attention, because of its large central velocity gradient and velocity dispersion: it is one of the best candidate among nearby galaxies to host a massive black hole (BH of the order of 10^7-10^8 $M_\odot$, e.g. Kormendy & Richstone 1995). Possible scenarii include one massive BH, two BHs, or no BH at all. We will consider here only the first class of models, with several possibilities to account for the observed asymmetries. Previous studies already discarded a gravitational lens or a dust component to be responsible for these asymmetries (e.g. BEMN94), so we will discuss the two remaining ones: a dense stellar cluster falling into the nucleus (already suggested by Dressler & Richstone 1988, see also Lauer et al. 1993, BEMN94) or a thick eccentric disc of stars on Keplerian orbits around the black hole, maintained through self-gravity and dynamical friction on the bulge (Tremaine 1995).

2.1. Is the disc eccentric ?

Tremaine (1995) recently proposed a model based on a set of aligned Keplerian orbits, forming an $m = 1$ pattern. The main argument for an orbit crowding effect is the lack of any significant colour gradient between P1 and the rest of the nucleus, except for P2 which has a higher UV upturn which could correspond to the radio source detected by Crane et al. (1992) and linked with the presumed central dark mass. But as argued by King et al. (1995), this difference in the UV flux is equivalent to a single PAGB star, although it seems more extended (P. Crane, priv. comm.). Tremaine (1995) also argued that the observed isophote twist of P1 as well as the elongations of P1 and P2 along the P1-P2 axis are natural consequences of the eccentric disc hypothesis. The only problem in Tremaine's model lies in the strong predicted asymmetry of the observed velocity field, in contradiction with the recently acquired data of Kormendy (SIS/CFHT, $\sigma_\star \sim 0\farcs27$).

In his proposition, Tremaine (1995) suggests that the alignment of apsides of the orbits forming the eccentric disc is maintained by the self-gravity of the nuclear disc. In fact, an $m = 1$ mode could amplify in the disc, if it has a positive pattern speed Ω_p, and if dynamical friction against the non-rotating bulge removes effectively the angular momentum, provoquing more eccentricity in the disc orbits. The efficiency of this mechanism is still unknown.

2.2. An $m = 1$ density wave

Another possibility is that the $m = 1$ perturbation is transient, but slowly damped. Weinberg (1994) shows that a stellar system can sustain weakly damped $m = 1$ mode for hundreds of crossing times. A fly-by encounter could excite such a mode, and explain off-centring in some spiral galaxies. We have tried to estimate the relevant time-scale for the fading of an $m = 1$ excitation in the particular conditions of the M31 nucleus, in the presence of a massive black hole. The excitation was provided by a slight initial displacement of the black hole, either in space or velocity. An $m = 1$ spiral wave was generated in the nuclear disc (see Fig. 1), which disappeared through phase mixing in about 0.5 Myr, while the black hole was braked down to the centre by dynamical friction. The perturbation kept a positive pattern speed Ω= 50km/s/pc during about 3-4 rotations (the corresponding period is 0.125 Myr). After that only a material arm was precessing at the negative velocity Ω= -3.6km/s/kpc until 1 Myr. Finally, an unstable $m = 1$ mode may also exist in the presence of gas in the centre of M31 (Shu et al, 1990, Junqueira & Combes 1996).

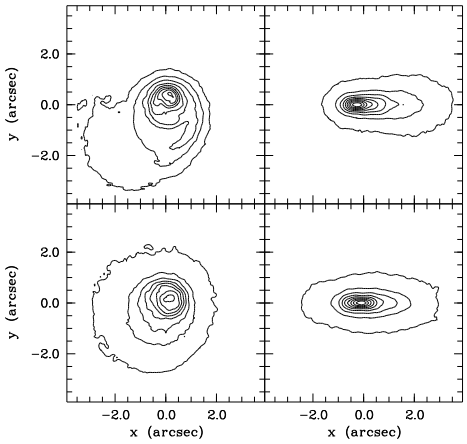

Fig. 1. Projected isophotes of the nuclear disc with the black hole launched with an initial offset. Left:face-on, Right:edge-on; Top: 0.08 Myr; Bottom: 0.32 Myr.

2.3. A falling stellar cluster

Even at HST resolution, the nucleus of M 31 appears as the superposition of two rather smooth components corresponding to P1 and P2. The detailed structure of each individual components depends on the decomposition method (BEMN94, King et al. 1995) but the corresponding global parameters seem to vary very little (see Table 1). Let us emphasize, as already did King et al. (1995), that although the brightest point of the nuclear region of M 31 corresponds to P1, it never contributes more than 0.55 of the total surface brightness (assuming P2 is symmetric) and the integrated magnitude of P1 is 2.6 magnitude fainter than of P2. Occam's razor suggests

Table 1. Global parameters for P1 and P2: absolute magnitude in the V band, core radius, mean ellipticity, relative position angle (PA in degrees), and displacement (in arcsecond) along the nucleus major ($\delta x'$) and minor-axis ($\delta y'$).

#	M_V (mag)	r_c ($''$)	$\langle\epsilon\rangle$	$\langle$PA$\rangle$ ($^\circ$)	$\delta x'$ ($''$)	$\delta y'$ ($''$)
P1	-9.6	0.25	0.31	104	-0.5	0.14
P2	-12.2	0.88	0.39	54	0	0

to favor the hypothesis of P2 being a nearly symmetric system, and P1 a superimposed elongated cluster. Since the velocity profile does not seem to be highly perturbed by the presence of P1 (even at the resolution of $\sigma_\star \sim 0''.27$ attained by SIS data), it suggests that the line-of-sight velocity of P1 is close to the line-of-sight velocity of the surrounding nuclear stars (including the seeing effect). In this scenario, the main effect is due to the low dispersion of the superimposed cluster which produces the offset observed in the velocity dispersion field (BEMN94). We examine this point in details in Sects 4 and 5.

3. N-body models

3.1. The code

We have simulated the infalling of a compact stellar system in the nucleus of M 31 using an N-body code whose main characteristics were described in Combes et al. (1990). A 3D cartesian grid was used, with free boundary conditions, and we used the method described by James (1977) to avoid a 2^3 multiplication of the number of cells in the grid. The total number of particles was 152384, and the grid size $128 \times 128 \times 80$. The time step of integration was 200 yr.

3.2. Initial conditions

As already suggested by Lallemand (1960), the nucleus of M 31 appears as a distinct photometric and dynamical component. Indeed, observed properties of the galaxy exhibit strong changes as we reach a radius of about 3 arcseconds along the major-axis:

- the surface brightness rises by more than 1.5 magnitude in the central 2 arcseconds, while the outer major-axis profile of the bulge only shows an increase of 0.1 magnitude in the same interval.
- the stellar velocity is nearly zero at 3 arcseconds but peaks around 155 km.s^{-1}at $0''.8$ ($\sigma_\star \sim 0''.27$, Kormendy & Richstone 1995, hereafter KR95).
- the stellar velocity dispersion stays nearly constant in the inner bulge with $\sigma \sim 150$ km.s^{-1}, and starts to rise in the inner 2 arcseconds to reach a value of ~ 250 km.s^{-1}(KR95) in the centre.

Moreover, Bacon et al. (1994) have shown that the assumption of the nucleus being a dynamically isolated entity leads to differences of less than 1% in the derivation of a local tensor virial theorem. This encouraged us to treat the bulge and the nucleus as two separate components. We therefore adapted the grid to the size of the nucleus[1], by taking a cell size of 0.165 pc which led to a volume of about $21 \times 21 \times 13$ pc^3 centred on P2.

3.2.1. The bulge

Since the nucleus appears as a dynamically isolated component, we include the contribution of the bulge as a fixed potential[2].

We have assumed the bulge to be spherically symmetric in our simulations. This assumption leads to an error of less than 10% in the potential of the bulge inside the volume of the grid. Moreover, in the presence of a supermassive black hole of a few 10^7 M$_\odot$, this error is negligible in the central part of the nucleus. We thus approximated the mass density distribution of the bulge by a sum of Plummer spheres of different masses and scales: these functions yield simple analytic formula for the corresponding gravitational potential and forces.

$$\rho\,(r) \;=\; \sum_i \left(\frac{3M_i}{4\pi b_i^3}\right) \times \frac{1}{\left(1+\frac{r^2}{b_i^2}\right)^{-5/2}} \qquad (1)$$

$$\Phi\,(r) \;=\; -\sum_i \frac{GM_i}{\sqrt{r^2+b_i^2}} \qquad (2)$$

where M_i and b_i are the total mass and the scale of the $i^{\rm th}$ component respectively. We have fitted the luminosity profile of the bulge using the axisymmetric model of BEMN94 (see Table 11) and the data of Kent (1983). This was achieved with a set of 4 Plummer spheres whose parameters are given in Table 2. Fig 2 shows the excellent

[1] Throughout this paper, we use a distance of 0.77 Mpc for M 31 which leads to a scale of $1'' \sim 3.73$ pc.

[2] Note that the definition of the "bulge" depends on the decomposition method. We rely here on the bulge/nucleus decomposition given in BEMN94.

agreement between this model and the published data on the inner bulge. The fact that we include the bulge

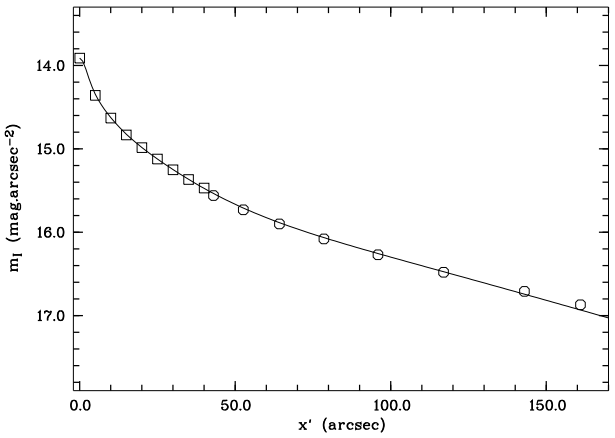

Fig. 2. Major-axis surface brightness profile in the I band of the fixed bulge compared to the inner axisymmetric bulge model of Bacon et al. (1994, squares), and the values given by Kent outside $40''$ (circles, rescaled for the I band).

Table 2. Parameters of the Plummer spheres for the bulge component: total mass (M_i), Plummer scale (b_i) and the integrated mass inside a sphere of 10 pc (M_i^{10}).

i	M_i ($M_\odot$)	b_i (pc)	M_i^{10} ($M_\odot$)
1	$3.7\ 10^7$	16.5	$5.2\ 10^3$
2	$3.0\ 10^8$	55	$1.7\ 10^3$
3	$3.3\ 10^9$	176	$6.0\ 10^2$
4	$3.7\ 10^{10}$	770	$8.1\ 10^1$

contribution through a fixed potential allowed us to use all 152384 particles for the nucleus and the falling stellar cluster. Following BEMN94, we fixed the total visible mass of both components to $1.9\ 10^7$ $M_\odot$, leading to a mass of ~ 125 $M_\odot$per particle. The mass of the bulge inside the grid can easily be derived with the formula: $M(r) = \sum_i M_i r^3/(r^2+b_i^2)^{3/2}$. Inside $r = 10$ pc the bulge contributes for a mass of $\sim 7.6\ 10^3$ $M_\odot$, which is negligible compared to the added masses of P1 and P2.

3.2.2. The nucleus

The nucleus is represented by 138530 particles ($\sim 91\%$ of the total number), with an equivalent mass of $\sim 1.73\ 10^7$ $M_\odot$. We simulated it as a Toomre disc of size 3.8 pc. The vertical structure follows initially a sech^2 distribution with a vertical scale of 1.7 pc at the origin, and slightly increasing with radius to fit the observed photometry. The radial variation of height with radius was chosen as $(1+(r/9pc)^2)^{0.35}$. The radial velocity dispersion is taken as an exponential law, to better approach the data:

$$\sigma_r = \sigma_0 exp(-r/r_v)$$

with σ_0=280km/s, and r_v = 5pc. The azimuthal dispersion is taken, following the epicyclic approximation, as $\sigma_\theta = \sigma_r \frac{\kappa}{2\Omega}$. Since the potential is nearly spherical towards the centre due to the presence of the massive black hole that dominates the mass, a first approximation of the z dispersion is to take it equal to the radial dispersion $\sigma_z = \sigma_r$. However, since this choice was not enough to keep, after relaxation, a nucleus as thick as observed, our final choice for the nearly edge-on nuclear disc was $\sigma_z = 1.3\sigma_r$. The actual rotational velocity was computed, after subtracting the asymmetric drift, according to Jeans equations (cf Binney & Tremaine 1987).

3.2.3. The stellar cluster

The stellar cluster is represented with the remaining 13854 particles (9% of the particles corresponding to $\sim 1.73\ 10^6$ $M_\odot$), as a truncated Plummer sphere with an equivalent core radius $r_c = 0.13$ pc (initial r_c to anticipate any evolution). The tidal radius R_t of the stellar cluster is adjusted to its initial environment, since it is launched at a radius R_0=6-9pc from the centre (R_t is between 1.6 and 2.2pc). The resulting concentrations $c = \log(R_t/r_c) \approx 1-1.2$, fall within the whole range of concentrations observed for globular clusters in our Galaxy (0.75 to 1.75). The velocities follow an isotropic maxwellian distribution truncated at the escape velocity, and with a temperature parameter, providing the amount of kinetic energy corresponding to the virial theorem.

The cluster is launched in the equatorial plane (at the radius R_0=6-9pc) with the velocity V_0 (see Table 3). In most of the experiments, V_0 corresponds to the circular velocity at R_0. This was motivated by two facts: first that dynamical friction does not depend much on the orbit history of the satellite (e.g. Lin & Tremaine 1983) provided it is not yet disrupted. Since the central density of the cluster is an order of magnitude higher than 10^5 $M_\odot$ pc^{-3}, the average density within 6pc including the black hole, we know that the tidal disruption has not occured at this radius (only the envelope of the cluster has been stripped away, which is taken into account through the initial R_t). And second, dynamical friction has the tendency to circularise orbits (Bontekoe & van Albada 1987). However, we have in Sect. 4 also performed experiments with a cluster on an hyperbolic orbit: this will give us insights for the particular case of M31's nucleus (see Sect. 5).

3.2.4. The black hole

The observed steep central velocity gradient and velocity dispersion peak suggested the presence of a central

dark mass of a few 10^7 $M_\odot$(Dressler & Richstone 1988, Kormendy 1988). Bacon et al. (1994) confirmed this result with self-gravitating two-integral dynamical models of the nucleus of M 31, and derived a central dark mass of $\sim 7.10^7$ $M_\odot$. We model it with a Plummer sphere with a core radius $r_c = 0.13$ pc (i.e. limited by our resolution of 0.15 pc) and a mass of a few times 10^7 $M_\odot$(see Table 3).

3.3. Initial parameters

We restrict our analysis to some of the parameters we thought to be crucial for the evolution of the system (cf Table 3):

- the black hole mass M_{bh},
- the mass-to-light ratio of the cluster $(M/L)_C$ (i.e. its mass),
- the initial radius of the cluster R_0.
- the initial velocity of the cluster V_0.

Table 3. Parameters of the different experiments: the black hole mass M_{bh} ($M_\odot$), the ratio between the M/L of the nucleus and the cluster $\eta(M/L)$, the core radius of the cluster r_c (pc), the radius R_0 (pc) and velocity V_0 (km.s^{-1}) at which the cluster is launched.

run	M_{bh}	$\eta(M/L)$	r_c	R_0	V_0
#1	6.5 10^7	1	0.12	8.8	V_c
#2	9.0 10^7	1	0.12	6.6	V_c
#3	1.1 10^8	1	0.12	6.6	V_c
#4	1.1 10^8	2	0.12	6.6	V_c
#5	1.1 10^8	1	0.12	6.6	$1.5 \times V_c$
#6	1.1 10^8	1	0.12	6.6	V_c
#7	1.1 10^8	1	0.12	6.6	$-V_c$
#8	1.1 10^8	1	0.12	6.6	V_z
#9	2.2 10^7	1	0.12	6.6	V_c

4. The disruption of the cluster

If P1 indeed corresponds to an additional cold stellar system and is spatially close to the centre of the nucleus, its decaying time should be rather short, and the probability to observe such a configuration is very small. This is the main argument against the falling cluster hypothesis. However Lauer et al (1993) emphasize that the dynamical friction effects are not well known, and there exist some circumstances where it may shut off. They privileged the hypothesis of P1 being an external stellar system coming from another nucleus, possibly having its own central BH.

4.1. Dynamical friction

A simple application of the Chandrasekhar formula (see e.g. Binney & Tremaine 1987) can give us a first estimate of the falling time of a stellar cluster. For a system of 1.6 10^6 $M_\odot$, it would take a Hubble time to fall in the centre from a radius of a few kpc. This timescale is strongly dependent on the initial radius r_i, so that only $\sim 10^5$ yr are needed for the system to fall from a radius of 6.6 pc (with $V_{P1} \sim 300$ km.s^{-1}, see Table 3 and Sect. 5.1).

However, the application of the Chandrasekhar formula here is not appropriate. On one hand, this formula overestimates the dynamical friction since it assumes a singular isothermal sphere while P1 has entered the core where the density remains constant. Moreover, the gravitational potential is dominated by a central point-like mass, which does not provide friction.

On the other hand, our simulations confirm a much more important result already noticed in the case of interacting galaxies by Prugniel & Combes (1992): the Chandrasekhar formula underestimates the effect of dynamical friction since it assumes that the accreted system is rigid. Prugniel & Combes (1992) showed that releasing the hypothesis of a rigid satellite increases considerably the friction efficiency. In our experiments, the main dynamical friction is indeed due to the deformation of the stellar cluster, a reciprocal effect usually neglected in estimations based on the Chandrasekhar formula.

4.2. Tidal forces and the black hole mass

Our simulations show that the main effect is due to the tidal forces induced by the central mass concentration which rapidly disrupt the cluster. The strength of the tidal forces strongly depends on the ratio of the central cluster and nucleus concentrations. For a black hole mass of $\sim 6.10^7$ $M_\odot$, the cluster looses 30% of its mass in less than 10^5 yr. After 4.10^5 yr, they are all spread in a ring-like structure (Fig. 3), *although the centre of gravity of the cluster's particles is close to the centre of the nucleus*. For masses greater than 6 10^7 $M_\odot$, the black hole dominates the overall gravitational potential in the central 10 pc. The lifetime of the cluster is then roughly scaled like the inverse of the square root of the central dark mass (Fig. 4). We also ran an experiment equivalent to run #3 but without the additional central mass. In this run, the stellar cluster is not disrupted. On the contrary, it is the nucleus now that suffers strong tidal deformations, and the cluster decays like a rigid body through dynamical friction, produced by the nucleus deformations. The decay time is then longer, of the order of 3 10^5 yr.

In Fig. 3, we can also see that there is very little transfer of angular momentum between the nucleus and the original cluster: the mean angular momentum had only changed by 10% by the end of the simulation at 4.6 10^5 yr. This result is very similar to the one obtained by Charlton & Laguna (1995) at a larger scale: the debris of the globular clusters disrupted by tidal forces mainly follow the original cluster orbit (i.e. highly eccentric orbits).

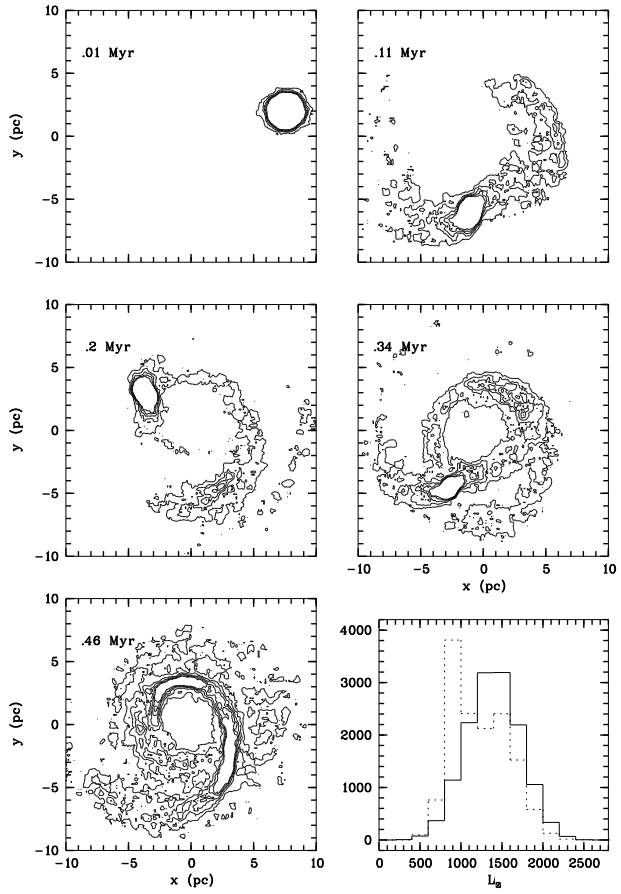

Fig. 3. Face-on view of the cluster particles at different times of the simulation (run #1): the surface brightness has been slightly smoothed and only the faintest contours have been drawn to emphasize the development of the ring-like structure. The bottom right panel shows the histogram of the angular momentum for the cluster particles at the begining and at the end of the simulations (0.01 Myr – solid line – and 0.46 Myr – dashed line – respectively).

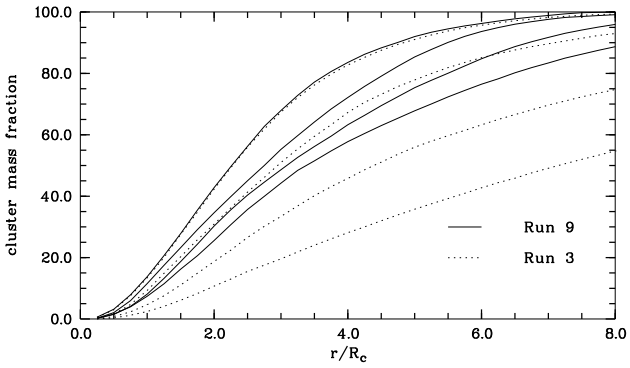

Fig. 4. Effect of the central mass concentration on the disruption of the cluster: the mass of the cluster (in % of its total mass) enclosed in a sphere of radius r (normalized by the initial core radius r_c) is shown as the simulation evolves (from top to bottom, $t = 10^4$, 2.10^4, 3.10^4 and 4.10^4), for two different central mass concentrations (2.10^7 $M_\odot$– solid lines – and 10^8 $M_\odot$– dotted lines).

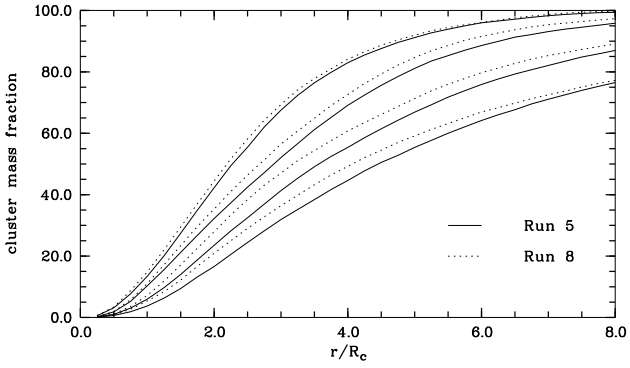

Fig. 5. Same as Fig. 4 but for two different initial velocities of the cluster: run #5 corresponds to a cluster on an hyperbolic orbit in the equatorial plane, and run #8 to an initial pure vertical velocity for the cluster. Note the difference with run #3 in Fig. 4.

In most runs presented in this paper, we have launched the cluster with the circular velocity. In run #5, we have launched the cluster with a tangential velocity of $1.5 \times V_c$ (hyperbolic orbit) and in run #8 with a purely vertical velocity of 250 km.s^{-1}. In both cases, the distance between the cluster and the central mass concentration increases with time. This prevents the cluster to be strongly disrupted as illustrated in Fig. 5 (see also Charlton & Laguna 1995).

4.3. The mass-to-light ratio of the cluster

Because of the absence of colour gradients, we assumed until now that P1 and P2 have similar stellar populations and mass-to-light ratios. We have however also explored different mass-to-light ratios (hereafter M/L). For the run #4, we fixed the M/L of the cluster to be half the one of the nucleus (see Table 3). This was achieved by assigning fewer particles to the cluster, which were then used for the nucleus whose total mass was conserved. The less massive cluster is obviously less concentrated at all times after the launch. However, its envelope seems to survive longer. To understand this point it is necessary to remember that the initial total energy of the clusters are different in those two runs: in run #3 the cluster covers a longer track which induces a larger spreading of the unbound particles. Moreover, the tidal radius of the cluster is significantly smaller (by about 25%) in run #4 than in run #3.

5. The case of M31 nucleus

5.1. Some simple geometrical arguments

Let us first assume that the stellar cluster is located in the equatorial plane of the (axisymmetric) nucleus, and let (x^c, y^c), (V_x^c, V_y^c) be its position and velocity in a reference system centred on P2 where Ox is the line of nodes. Since we observe P1 at about 0.″14 of P2 along the nuclear minor-axis and 0.″5 along the major axis (Lauer et al. 1993, BEMN94), we can write: $y^c = 0.''14/\cos i$ with i being the inclination angle of the nucleus ($90° \equiv$ edge-on). In this case, the nucleus of M 31 cannot be viewed exactly edge-on. The average axis ratio of the nucleus of $\langle q \rangle$ of 0.61 can be used to bracket its inclination angle: $\arccos(0.61) \sim 52.4 < i(°) < 90$. Then, the apparent distance of P1 to the major-axis of the nucleus provides us a lower limit for the true distance of P1 to the line of nodes: $y^c > 0.''14/0.61 \sim 0.''23$. And we have now $R^c = \sqrt{(x^{c2} + y^{c2})} > 0.''55$ ($\sim$ 2 pc at 0.77 Mpc). If the near side of the nucleus corresponds to the near side of the main disc of M 31, i.e. the North-West side (see Fig. 3 of Kormendy 1988), we can conclude from the sign of the observed velocities that P1 is going toward the line of nodes of the nucleus.

The projection on the sky gives $V_y^c = V_{los}^c/\sin i$, where V_{los}^c is the line-of-sight velocity of P1. If we assume now that the cluster is on a circular orbit, we can also write:

$$V^c(R) = \frac{V_y^c \times R^c}{x^c} \tag{3}$$

with V^c the spatial velocity of P1. Using Fig. 7 of Kormendy & Richstone (data of Kormendy & Bender 1995), we estimate V_{los}^c to be $\sim$ 160 km.s^{-1}(see Sect. 5). This value is very uncertain, but the following calculations can be adapted accordingly. The projected distance x' $(= x)$ along the nuclear major-axis is $\sim 0.''5$ (Lauer et al. 1993, BEMN94). Therefore $V^c(R) \sim 320 \cdot (\sqrt{(0.25 + y^{c2})}/\sin i)$. $V^c(R)$ is then minimum ($V^c \sim 211$ km.s^{-1}) for $i \sim 62.6°$ which gives $y^c \sim 0.''3$ and $R^c \sim 0.''59$.

In fact, since we already have observed values for x^c and V_{los}^c, we only need to get y^c (or the inclination i) and V_x^c to know the full position and velocity of the cluster. Using the model given in Bacon et al. (1994) for the spatial mass distribution and assuming a supermassive black hole of $M_{bh} = 10^8$ M$_\odot$(see Sect. 5), it is then possible to roughly constrain the type of orbit of the cluster in terms of these two unknowns y^c and V_x^c (as a test particle in a fixed potential). This is illustrated in Fig. 6, where the limits of the regions for elliptic, and hyperbolic orbits are drawn as well as the curves for tangential and radial velocities. We thus find that there is only one point where P1 can be on a circular orbit: $V^c \sim 300$ km.s^{-1}for $R^c \sim 1.05''$ and $y^c \sim 0.''9$ (see Fig. 6). Taking into account the uncertainty on the true value of V_{los}^c and on the circular velocity in the nucleus, Fig. 6 indicates that $0.85 < R^c('') < 1.3$ or $0.7 < y^c('') < 1.2$ ($2.6 < y^c(pc) < 4.5$ at 0.77 Mpc).

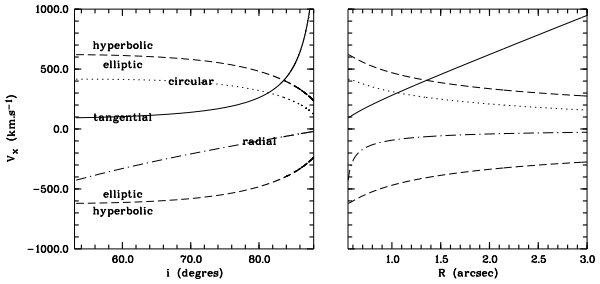

Fig. 6. Diagrams showing the different types of orbits for a test particle in the modelled potential of M 31 (see text) in terms of i (or R^c) and V_x^c: the dashed lines correspond to the escape velocity, the dotted line to the circular velocity. Geometrical constraints are given by the solid line (pure tangential velocity) and the dotted–dashed line (radial orbits). Vertical dotted lines indicate the circular velocity solution.

The core of the cluster could survive only if its central density is larger than the average mass density of the nucleus interior to its orbit. We have seen in the simulations that the initial central density of the cluster had to be $\approx$ 10 times the average density at $R_0 = 6$pc (including a black hole mass of 7 10^7 M$_\odot$). We therefore expect that the disruption will occur at a radius of $\sim$ 3 pc. This roughly corresponds to the radius derived for a circular orbit inside the nucleus. If the stellar cluster follows such an orbit it is then presently being disrupted. Such quasi circular orbits were tried, where the cluster was slowly spiraling in towards the centre because of dynamical friction. But the stripping of its outer parts was so effective that, although the center of mass of the system did reach the required radius, the remaining core of the globular cluster did not. Also, the disruption of the cluster produced a much too large internal velocity dispersion to the stellar debris around the core; the presently observed low velocity dispersion of P1 strongly suggests that this is not the case yet. Therefore, we must conclude that P1 cannot be on a circular orbit around P2.

Finally, for a central dark mass of 1. 10^7 M$_\odot$the circular velocity predicted from the model given in BEMN94 is smaller than 160 km.s^{-1}at radii larger than 0.″55. Therefore, if the mass concentration is smaller than 1. 10^7 M$_\odot$, the cluster is on an orbit unbound with respect to the nucleus, and will escape from its gravitational influence (and might eventually fall back later by friction).

We have not explored many different inclinations of the orbital plane. However, as the main influence comes from the central dark mass, the fate of the cluster is mainly determined from its pericentre distance.

5.2. Observations of the experiments

The main problem to fit self-consistently the nuclear disc of M31 is its observed thickness, mainly under the assump-

tion of its nearly edge-on inclination. This requires a relatively high z-dispersion, while the disc is highly rotating in the plane. The system relaxes quickly, on time scales of the order of 10^4 yr, and it revealed very difficult to maintain both a rather thick disc, and a high V_{rot}/σ ratio. With relaxation, the velocity dispersion tends to become more isotropic, and the rotational velocity decreases with respect to the in-plane dispersion. To reproduce the high azimutal velocities, a more massive black hole is required, and no good fit was obtained below 8 10^7 $M_\odot$.

We have "observed" the simulations by associating a specific luminosity of 50.5 $L_\odot$per particle as to reproduce the photometric data in the I band (i.e. $M/L_I \sim 2.5$). For the bulge, we used the axisymmetric surface brightness model given in BEMN94 (including the difference in position angle, see their Table 4). The system (nucleus + cluster) was viewed such as the strongest projected peak of the cluster is located at $x' = 1.85$ pc and $y' = 0.5$ pc from the centre of the nucleus (see BEMN94). This fixes the three Euler angles (ψ, θ, ϕ) of the projection. All the relevant characteristics of the various instrumental setups are then taken into account: spatial and spectral pixel sizes, spatial and spectral resolutions. The Point Spread Function was approximated by a single gaussian function which is thus completely fixed by its width $\sigma_\star$. For the bulge we assumed a gaussian Line Of Sight Velocity Distribution (hereafter LOSVD) whose first two moments are those of the corresponding isotropic axisymmetric model (i.e. Model A of BEMN94 with $M/L_I = 2.5$ and the appropriate central dark mass). The obtained total LOSVDs were parametrized with the help of Gauss-Hermite functions (see van der Marel & Franx 1993)

Let us first examine the hypothesis of a projection effect, where the cluster is physically far from the centre of M 31. The results of these experiments will be used to constrain a fully self-consistent simulation.

5.3. Stellar cluster seen in projection against the nucleus

Lauer et al. (1993) argued that the observed photometry and kinematics speaks against a cluster physically far from the centre and seen in projection:

- P1's luminosity profile is truncated and asymmetric: this is indeed suggestive of an interaction between P1 and P2. However, as mentioned by King et al. (1995), the decomposition is certainly not unique
- Lauer et al. (1993) also argued that the positioning of P1 on the nucleus major-axis favors a physical relationship between P1 and P2. But this assumes that P2 is seen almost edge-on. Moreover, P1 is closer to the major-axis of the bulge.
- The velocity profiles are symmetric, as though P1 did not introduce any perturbation. But this could come in part from the fact that the observed kinematics is luminosity weighted (seeing effect, cf Sect. 5.5).
- Lauer et al. (1993) estimated that the P1 velocity dispersion is too large for a globular cluster. However, the recent SIS data obtained by Kormendy indicate that $\sigma_{P1} < 85$ km.s^{-1}(KR95). Moreover, our simulations suggest (see Sect. 5.3.1) that $30 < \sigma_{P1}$(km.s^{-1}) < 80 (if P1 is being disrupted it is certainly not in virial equilibrium).

Although P1 and P2 seem to be interacting, there are thus no definite arguments against a projection effect. We will therefore examine this possibility in the following paragraphs, and use this to test the stability of the model, after a relaxation of several dynamical times.

The apparent flattening of the nucleus (see Sect. 5.1) sets a lower limit of $\sim 53°$ for its inclination angle. We have attempted to reproduce the photometry and the kinematics of M31 's nucleus using a thin disc and a central dark mass of a few 10^7 $M_\odot$. We managed to get a reasonable fit with $M_{bh} = 7.7\ 10^7$ $M_\odot$and an inclination of 55°. The cluster has been fixed as a separate Plummer sphere with $r_c = 0.8$ pc, projected onto the nucleus. The simulation of the nucleus has been continued until the system reached dynamical stability. Self-consistent experiments are described in Sect. 5.4.

In Fig. 7 we present the isophotes[3] of the model compared to the WFPC2 I band image kindly provided by Michael Rich. We normalized both images using the HRCAM I_c band image (BEMN94). The fit is rather good, although we do not reproduce the flattening of P1 as well as its full spatial extension (see King et al. 1995). Our nucleus is also slightly more peaked than in the observations. This is due to the fact that we start from conditions that are close to what is observed. Then dynamical relaxation is at work and the nucleus has a tendency to concentrate.

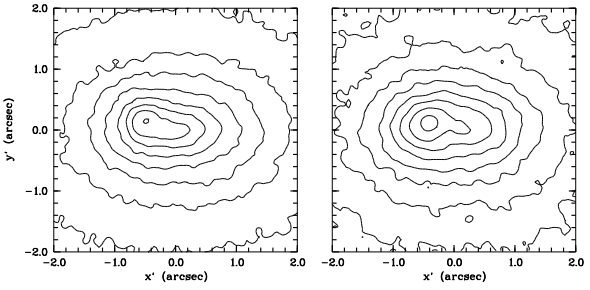

Fig. 7. I_c band isophotes of the "inclined" model (left panel) and of the WFPC2 I band image (normalized to the Cousin system, right panel). The brightest isophote corresponds to 11.85 mag.arcsec^{-2}, and the step is 0.3 mag.arcsec^{-2}.

[3] In all the following figures, we have aligned the nucleus major-axis with the horizontal axis: see BEMN94.

5.3.1. Comparison with published kinematics

As discussed above, the line-of-sight velocity of the cluster V^c_{los} suggested by the available observables is probably close to 160 km.s^{-1}. However, it is difficult to determine V^c_{los} with certainty. A way to constrain the mean value for V^c_{los} is to directly look at the influence of P1 on the LOSVDs. This has been already done by BEMN94 who unfortunately only examined a very limited subset of possibilities. Moreover, at the spatial and spectral resolution of the TIGER data ($\sigma_\star \sim 0\farcs38$) the light contribution of P1 is significantly diluted. BEMN94 still observed a slight asymmetry in the velocity curve along the nucleus major-axis which hinted for a rather high apparent value of V^{P1}_{los} (> 120 km.s^{-1}). We have fixed V^c_{los} to a number of different values to test for its effect on the shape of the resulting LOSVDs and the corresponding derived velocities and dispersions. The internal velocity dispersion of the cluster is assumed isotropic with $\sigma^c \sim 36$ km.s^{-1}.

For comparison we have used the kinematics obtained with the two-dimensional TIGER data presented by BEMN94 (spatial resolution of $\sigma_\star \sim 0\farcs37$ and spectral resolution of ~ 100 km.s^{-1}). The best fit is obtained for $V^c_{los} = 140$ km.s^{-1}but values of 120 and 160 km.s^{-1}are also consistent with the data (Fig. 8). Higher velocities for the cluster tend to increase both the peak in the velocity and velocity dispersion profiles, but to reduce the influence on higher order moments. It is important to remember that the kinematics were derived here from a gaussian fit to the LOSVDs, and that true statistical moments are less influenced by the presence of the cluster. Although Fig. 8 only shows the major-axis kinematical profiles, the agreement is excellent on the full two-dimensional fields. The higher resolution data of Kormendy (SIS/CFHT, $\sigma_\star = 0\farcs27$; KR95) also suggests a value of $V^c_{los} \sim 160$ km.s^{-1}, which will therefore be used for the "self-consistent" model (Sect. 5.4).

We have finally estimated the effect of a higher velocity dispersion of the cluster by increasing its mass by a factor of 2: this increases the internal velocity dispersion by a factor of $\sqrt{2}$. As expected the velocity profiles are almost coincident but the velocity dispersion profiles differ significantly: the minimum along the major-axis reaches ~ 95 km.s^{-1}for $\sigma^c = 36$ km.s^{-1}($M/L_I = 2.5$) and ~ 112 km.s^{-1}for $\sigma^c = 51$ km.s^{-1}($M/L_I = 5$) closer to the observed values. This suggests a reasonable interval for the internal dispersion of the cluster: $30 < \sigma^c(\mathrm{km.s^{-1}}) < 80$.

5.4. Stellar cluster inside the nucleus

We have then examined the case of a rather more edge-on model for the nucleus, but this time including the stellar cluster in a self-consistent way. In this case, the nucleus should be significantly thicker as the apparent flattening is closer to the true one, and we have chosen a z velocity dispersion slightly higher than the radial dispersion

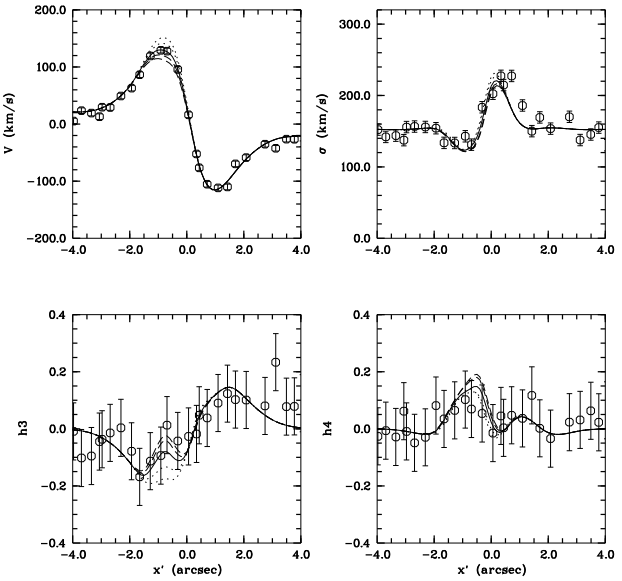

Fig. 8. TIGER velocity, dispersion, h_3, and h_4 major-axis profiles (circles). The corresponding profiles derived from the "inclined model" are presented for different values of V^c_{los}: 100 and 120 km.s^{-1}(dashed lines), 140 km.s^{-1}(solid line), 160 and 180 km.s^{-1}(dotted lines).

($\sigma_z = 1.3\sigma_r$, see Sect. 3.2.2). The nucleus is projected with an inclination $\sim 70°$. The orbit of the stellar cluster is no longer in the equatorial plane, but follows a nearly planar orbit, inclined by $\sim 20°$, so that the orbit is almost edge-on projected on the sky. We have already excluded a circular orbit (5.1), and therefore have chosen an hyperbolic orbit, the cluster being now very close to its pericenter of 3pc, where it has barely reached the critical radius of disruption.

We obtained a reasonable fit to the observables for a central dark mass of 9.4 10^7 M$_\odot$and an inclination of 68° (constrained by the observed position of the cluster). The cluster was launched at 8.8 pc from the centre with a velocity of 420 km.s^{-1}. The cluster has a strong effect on the stability of the nucleus: the outer parts gain energy and inflate, while the center becomes more condensed. This is difficult to anticipate in the initial conditions, and causes the main discrepancy between this model and the observables: the central surface brightness of P2 is larger in the model than in the HST photometry (Fig. 9). Also, the nucleus has the tendency to dynamically relax towards a more centrally concentrated and flattened system, due to the strong influence of the central dark mass. The latter completely dominates the gravitational potential in the inner few arcseconds and tends to symmetrize the dispersion tensor in the centre. We should note however that although P2 is too concentrated in the model it has the correct integrated magnitude.

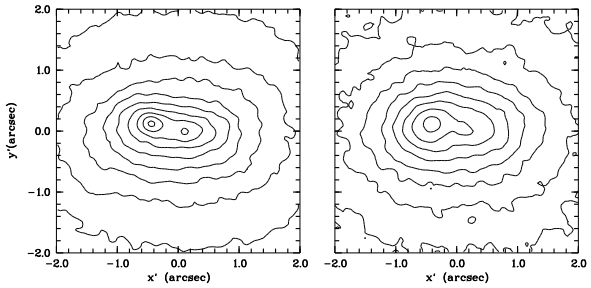

Fig. 9. Same figure as Fig. 7 but for the "self-consistent" model.

Figs. 10, 11, 12 and 13 present the comparison of this model observed at $t = 1.6\ 10^4$ years after the launch of the cluster with the TIGER and SIS data. The agreement is rather good even for the higher order Gauss-Hermite moments h_3 and h_4 (Fig. 10). As mentioned above, the isophotes are slightly too flattened which leads to a higher central surface brightness than in the observed image. At

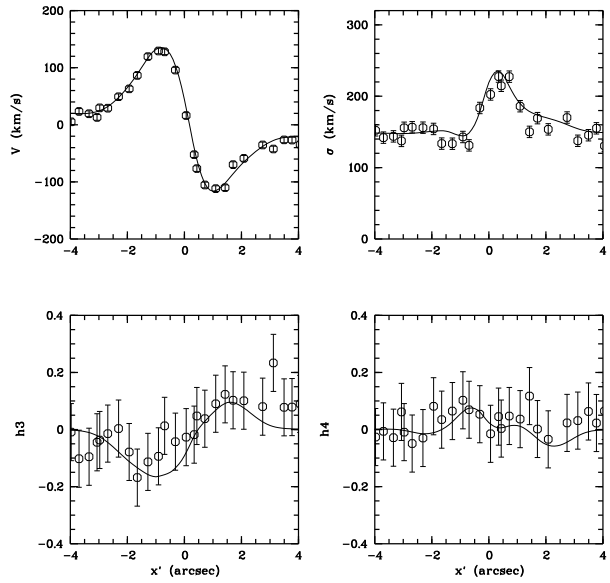

Fig. 10. Same as Fig. 8 but for the self-consistent" model.

a time $t = 1.6\ 10^4$ years, the cluster which lies at about 1.″1 (4.1 pc) is already partially disrupted, although the core still survives with a projected FWHM of $\sim 0.''4$. This is slightly smaller than the value of 0.″5 FWHM derived by King et al. (1995). The spread of the particles of the cluster induced by the tidal forces is accompanied by the creation of a large internal velocity gradient which in projection goes from ~ -105 km.s^{-1}to ~ 240 km.s^{-1}. This dilutes the contribution of the cluster to the observed LOSVDs.

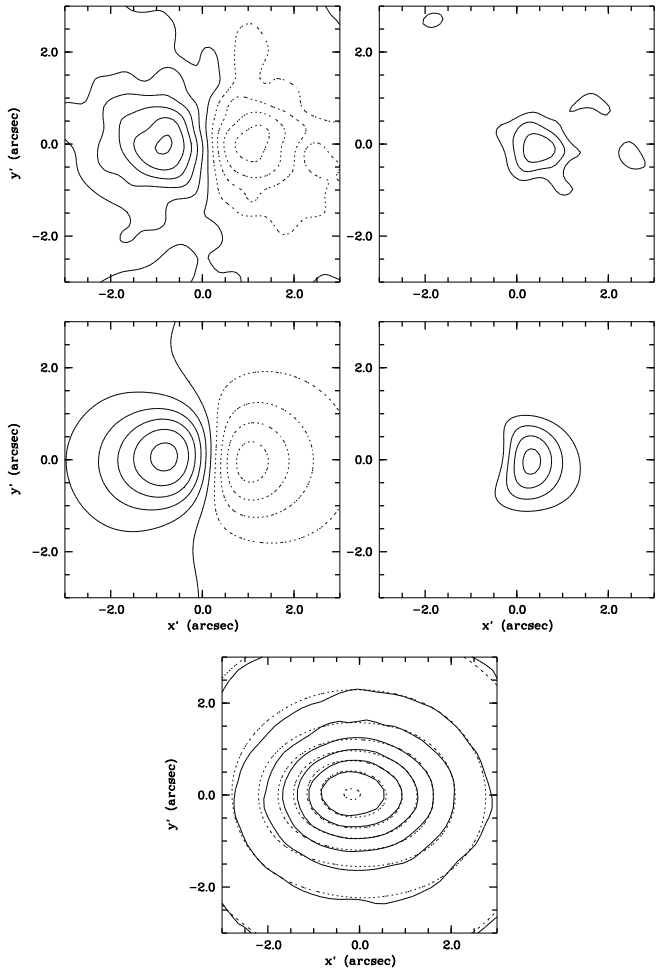

Fig. 11. Isophotes (bottom), velocity fields (left panels) and velocity dispersion fields (right panels) from the TIGER data (top panels) and of the "self-consistent model" (middle panels). The steps are respectively 0.25 magnitude, 25 km.s^{-1}(V) and 15 km.s^{-1}(σ).

5.5. M 31 at the HST resolution

At the HST resolution, the observed kinematics of the nucleus of M 31 should clearly reveal the presence of a superimposed cold cluster. This is illustrated in Fig 15 where we have derived the kinematics of the "self-consistent model" assuming a pixel size of $0.''06 \times 0.''06$. We also present seven corresponding LOSVDs along the line joining P1 and P2 for squared apertures[4] of 0.″26 and 0.″09 and a spectral resolution of 100 km.s^{-1}. Note the large wings of the LOSVD at the central position due to the presence of the mass concentration. There are no significant differences between the observed LOSVDs for the two different apertures. The velocity (gaussian fit) along the major-

[4] These parameters were chosen to be similar to the characteristics of the observations of M 31 with the HST Faint Object Spectrograph.

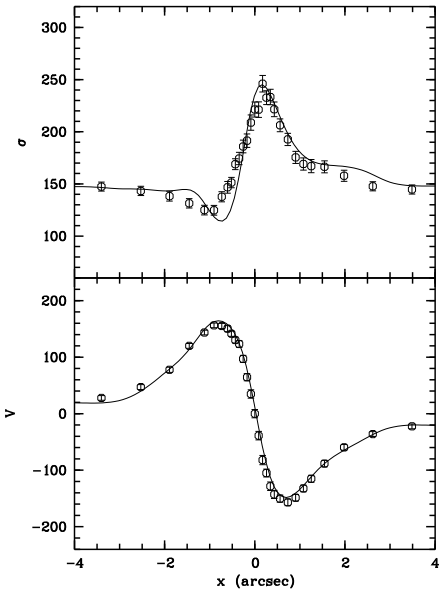

Fig. 12. Velocity and velocity dispersion of the SIS data (circles, KR95 and of the "self-consistent model".

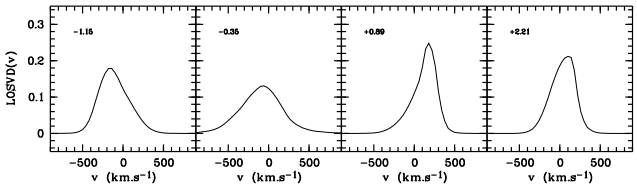

Fig. 13. LOSVDs derived from the "self-consistent model" at four different positions to be compared with Fig. 7 of KR95.

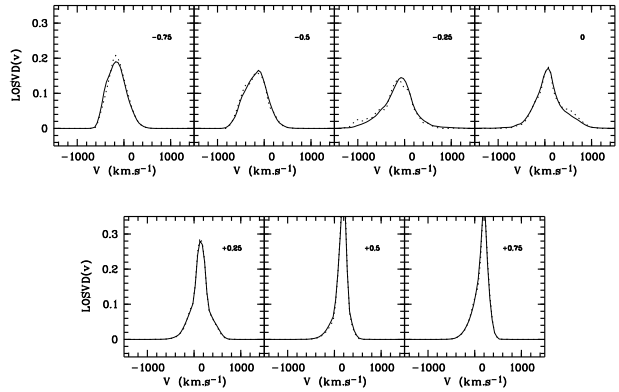

Fig. 14. LOSVDs from the "self-consistent model" at $-0\farcs75$, $-0\farcs5$, $-0\farcs25$, 0, $+0\farcs25$, $-0\farcs5$, $+0\farcs75$ along the P1/P2 line for squared apertures of $0\farcs26$ (solid lines) and $0\farcs09$ (dotted lines).

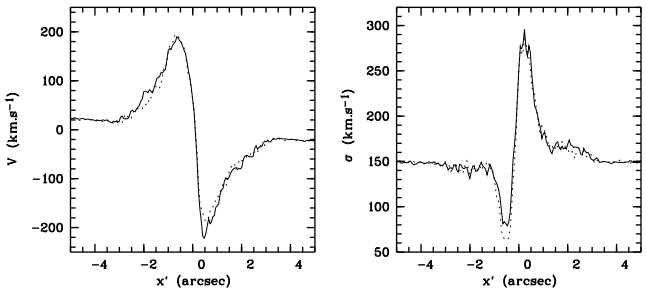

Fig. 15. Velocity (left) and dispersion profiles (right) along the major-axis of the nucleus (solid lines) and along the P1/P2 line (dotted lines) predicted from the "self-consistent model".

axis reaches ~ -220 km.s^{-1}on the side opposite to P1 at $\sim 0\farcs45$, and the maximum dispersion is ~ 290 km.s^{-1}at $\sim 0\farcs25$. The maximum positive velocity and the minimum dispersion obviously strongly depend on the true internal kinematics of P1. The main prediction for spectrographic observations at the HST resolution is the strong asymmetry in the velocity profile along the P1-P2 line, which is also clearly revealed in the shape of the LOSVDs. However, whatever P1 corresponds to (a stellar cluster or a density perturbation), the fact that the observed kinematics is weighted by light induce strong asymmetries. Finally, as noticed by Lauer et al. (1993), if the cluster has indeed a transverse velocity of ~ 440 km.s^{-1}as in the "self-consistent model" presented here, its proper motion should be $\sim 10^{-3}$ arcsecond in 10 years.

6. Discussion and conclusions

In this paper we have presented N-body simulations of a stellar cluster falling towards a galactic nucleus. These experiments were designed to ressemble the central region of M 31. First we have shown that it was possible to obtain reasonable fits to all observables, either with a projected stellar cluster (which served to adapt our initial conditions for the N body simulations), or with a stellar cluster close to the nucleus and interacting with it. The best model considered an initial orbit where the cluster was unbound to the nucleus. Slight discrepancies between this model and the data still remain (e.g. the nucleus isophotes flattening). This solution is certainly not unique and other significantly different initial conditions (e.g. the choice of the orbit) could lead to very similar observables.

Second, we have shown that the dynamical friction is even more efficient than previously estimated: the cluster rapidly decays to smaller distances, where it is disrupted through tidal interaction with the BH. The lifetime of such a cluster is short ($< 5\ 10^5$) at radii smaller than ~ 10 pc if a central dark mass of a few 10^7 M$_\odot$is present at the centre. The main argument against the scenario of a falling cluster is that we must see the M31 nucleus at a very special time. However, the decaying of a stellar cluster is not a rare phenomenon. Tremaine et al (1975) proposed that the falling of globular clusters could even be the formation mechanism of the nuclear disc. Orders of magnitude are consistent with the observations, if about 25 clusters have

been disrupted to form the nucleus, which mass has grown as $t^{1/2}$. This means that one cluster is falling every 400 Myr; since it will perturb the brightness distribution during ≈ 0.2 Myr, the probability of the present configuration of the M31 nucleus is about $4\ 10^{-4}$. This however includes only globular clusters spiraling in on a quasi-circular orbit. We have shown that P1 being on a circular orbit is inconsistent with the presence of a central dark mass of a few 10^7 $M_\odot$. More rapid globular clusters, in hyperbolic orbits, as in one of the scenarii proposed here, would be disrupted, but not slowed down enough to contribute to the nucleus mass.

Therefore, we should conclude that the hypothesis of a falling cluster (e.g. nucleus of an accreted dwarf galaxy, globular cluster) remains a viable explanation. Lauer et al. (1993) suggested that P1 could survive close to the centre if it contains a secondary black hole of "substantial mass". The probability of seeing it now in this configuration is even smaller than for a stellar cluster, given the frequencies of black holes. Only if we assume that dark matter in galactic halos is constituted by BHs are the latter more numerous than globular clusters. In the model of Lacey & Ostriker (1985), one of these 10^6 $M_\odot$ BH arrives in the centre every 10^8 yrs, and most of the time it merges with the BH already present, or is ejected if there is already a binary BH. Xu & Ostriker (1994) argue that, since fresh BH arrive regularly on the centre, the probability to find a binary BH with a separation of 1.6pc (as P1-P2) is 10%. It is however difficult to explain why P1 is so bright, without any cusp contrary to P2. More stringent is the constraint of a low dispersion at P1: in the case of a secondary black hole at P1, the dispersion there should be significantly larger than observed.

Our simulations finally served to precise the required BH mass, in the hypothesis of an axisymmetric nucleus: in order to fit the disc thickness and stability requirements, we need the presence of a mass concentration of at least $7\ 10^7$ $M_\odot$to explain the central stellar velocity and velocity dispersion gradients. The detection of a strong central UV and X ray source in the centre of M 31 is also in favor of a supermassive black hole. The main underlying assumption in the kinematical determination of the central dark mass is the *axisymmetry of the nucleus*. In a forthcoming paper, we will examine the possibility of a triaxial morphology (i.e. a bar) for the nucleus of M 31.

Acknowledgements. The authors would like to thank Roland Bacon for fruitful discussions, Nicolas Cretton, Frank van den Bosch and Luis Aguilar for their comments and suggestions, as well as Michael Rich for communication of data prior to publication. Simulations have been carried out on the CRAY computers of the IDRIS-CNRS center, in Orsay, France.

References

Bacon, R., Emsellem, E., Monnet, G., Nieto, J.L., 1994, A&A, 281, 691 (BEMN94)
Binney J., Tremaine S., 1987, in: Galactics Dynamics, Princeton series in Astrophysics, Ostriker J. ed.
Bontekoe, Tj., R., van Albada, T., S., 1987, MNRAS 224, 349
Charlton J.C., Laguna P., 1995, ApJ, 444, 193
Combes F., Debbasch F., Friedli D., Pfenniger D., 1990, A&A, 233, 82
Crane, P. C., Dickel, J. R., Cowan, J. J., 1992, ApJ, 390, L9
Dressler A., Richstone D.O., 1988, ApJ, 324, 701
James R.A., 1977, J. Comput. Phys. 25, 71
Junqueira S., Combes F., 1996, A&A 312, 703
Kent S.M., 1989, AJ, 97, 1614
King, I., Stanford, S. A., Crane, P., 1995, AJ 109, 164
Kormendy J., 1988, ApJ, 325, 128
Kormendy J., Richstone, D., 1995, ARAA, 33, 581 (KR95)
Lacey, C.G., Ostriker, J.P., 1985, ApJ 299, 633
Lallemand A., Duschene M., Walker M.F., 1960, PASP, 72, 76.
Lauer T.R., Faber S.M., Groth E.J. et al: 1993, AJ, 106, 1436
Light E.S., Danielson, R.E., Schwarzschild, M, 1974, ApJ, 194, 257
Lin, D., N., C., Tremaine, S., 1983, ApJ 264, 364
Prugniel P., Combes F., 1992, A&A, 259, 25
Shu F.H., Tremaine S., Adams F.C., Ruden S.P., 1990, ApJ, 358, 495
Tremaine S. D., 1995, AJ, 110, 628
Tremaine S. D., Ostriker, J. P., Spitzer Jr., L., 1975, ApJ, 196, 407
van der Marel, R. P., Franx, M., 1993, ApJ, 407, 525
Weinberg, M.D., 1994, ApJ 421, 481
Xu, G., Ostriker, J.P., 1994, ApJ 437, 184

This article was processed by the author using Springer-Verlag LaTeX A&A style file *L-AA* version 3.